

The Rotary Flexible Joint – A Holistic View from Modeling and Control to Observer Design and Experiments

Simon Helling,* Thomas Meurer*

* Automation and Control Group, Faculty of Engineering, Kiel University, (email: {sh,tm}@tf.uni-kiel.de)

Abstract: A two degrees of freedom (2DOF) control for a lab-scale vertically-mounted rotary flexible joint is addressed to realize a benchmark example for nonlinear control education and experimentation. To this end, the mathematical model is derived based on the Euler-Lagrange equations. Further insight into the model is given by addressing the relationship between the two translational springs and their approximation as a single torsion spring. The model is known to be differentially flat, which facilitates a feedforward control design by means of the flat parameterization. Furthermore, a state-feedback controller is introduced to stabilize the desired trajectory. State information is reconstructed using a Luenberger-type observer. Both the state-feedback controller and the Luenberger-type observer are designed based on a linear time-varying (LTV) approximation obtained using a linearization around the flat state parameterization of the system. The 2DOF design is illustrated using experimental results.

Copyright © 2023 The Authors. This is an open access article under the CC BY-NC-ND license (<https://creativecommons.org/licenses/by-nc-nd/4.0/>)

Keywords: Nonlinear control, feedback control, feedforward control, observers, pole assignment

1. INTRODUCTION

The rotary flexible joint is used as a benchmark model for robot links in several applications such as industrial robotics, satellite robot arms (Book, 1983), teaching (Quanser, 2012), and medical surgery robots (Riviere et al., 2003). Current research on the control of the rotary flexible joint is focused on PID controllers (Akyuz et al., 2011; Bilal et al., 2017), and Reinforcement Learning (Sendrescu et al., 2020). Nonlinear approaches often use feedback linearization (Markus et al., 2012; Didam et al., 2012; Markus, 2016), sliding mode control (Rsetam et al., 2020), or optimization-based techniques see, e.g. (Dharavath and Ohri, 2021). The device is widely-used for academic research and, as current research indicates, can be used as an illustrative testbed to teach a variety of different concepts from modeling, and system identification to concepts of linear and nonlinear control and state estimation.

Thus, we take the rotary flexible joint as a means to study the modeling process and nonlinear control design of the aforementioned setup. Most of the aforementioned methods rely on the availability of the full system state. However, none of the above-mentioned references relying on this information implement a state observer. Therefore, in this contribution a state observer is designed that reconstructs full state information. Furthermore, the potential energy of the rotary flexible joint is usually modeled by means of a torsion spring when, in fact, there are actually two translational springs. In this contribution, we address these issues by giving further insight into the relationship between the translational and torsion spring model. Moreover, we derive the mathematical model and the flat state and input parameterization of the rotary

flexible joint and, based on this construct a 2DOF control scheme that consists of a trajectory generator, a flatness-based feedforward controller, a stabilizing state feedback controller, and a Luenberger-type observer. The latter two make use of the flat parameterization of the system states in order to linearize the nonlinear dynamics to obtain a linear time-varying (LTV) model. Based on this simplified model, the state feedback controller and Luenberger-type observer can be designed using the Ackerman formula, see (Ackermann, 1972; Wiberg, 1971).

This article is structured as follows. In Sec. 2, the mathematical model of the rotary flexible joint is introduced using the potential energy of the two translational springs. Furthermore, the model simplification is derived based on the relationship between the translational spring forces and the torsion spring moment. Additionally, the flat parameterization of states and input is derived based on the system's output. In Sec. 3, the 2DOF control scheme is discussed including the trajectory generation, feedforward control, state (difference) observer, and state feedback control. Sec. 4 illustrates the proposed control scheme by means of an experimental setup for a swing-up of the rotary flexible joint which can be used as a testbed for students to learn about a variety of different methods in control theory. In Sec. 5 concluding remarks are given.

2. MATHEMATICAL MODEL

The rotary flexible joint setup, its geometric relations and coordinate conventions are shown in Fig. 2. A spring-loaded beam B is mounted on top of a platform P , where the springs connect both elements. The beam consists of a main arm and a load arm, where $m_{B,i}$, $l_{B,i}$, $i = 1, 2$ are their respective mass and length. Furthermore, $l_{M,2}$



Fig. 1. Photograph of the experimental setup in the horizontally-mounted position.

denotes the distance to the middle of the load arm ($i = 2$) measured from the entire beam's joint to the platform, and l_G is the distance to the center of gravity (COG) of the beam. The platform and beam deflection are given by the angles φ_P and φ_B , respectively. The platform P is actuated by a DC motor, which is controlled by an input voltage. The deflection angle of the beam w.r.t. the inertial coordinate system, i.e., $y = \varphi_P + \varphi_B$ can be measured. In the following, the equations of motion are derived using the Euler-Lagrange formalism, i.e.,

$$\frac{d}{dt} \frac{\partial}{\partial \dot{q}_j} L - \frac{\partial}{\partial q_j} L + \frac{\partial}{\partial \dot{q}_j} R = Q_j^{nc}, \quad j = 1, \dots, n \quad (1)$$

with the Lagrange function $L = E_{\text{kin}} - E_{\text{pot}}$ including the kinetic and potential energies E_{kin} and E_{pot} , respectively. Furthermore, $\mathbf{q} = [\varphi_P, \varphi_B]^\top$ are the generalized coordinates, $\dot{\mathbf{q}} = [\dot{\varphi}_P, \dot{\varphi}_B]^\top$ are the generalized velocities, R is the Rayleigh dissipation function, and $\mathbf{Q}^{nc} = [Q_1^{nc}, Q_2^{nc}]^\top$ are the generalized, non-conservative forces.

2.1 Equations of Motion

Consider the vectors from the inertial coordinate frame to the springs' fix-points given by

$$\mathbf{p}_0^a = R_0^P \mathbf{p}_P^a, \quad \mathbf{p}_0^b = R_0^P \mathbf{p}_P^b, \quad \mathbf{p}_0^c = R_0^B \mathbf{p}_B^c, \quad (2)$$

with vectors $\mathbf{p}_P^a = [l_x^a, -l_y^a, 0]^\top$, $\mathbf{p}_P^b = [l_x^b, l_y^b, 0]^\top$, and $\mathbf{p}_B^c = [l^c, 0, 0]^\top$. The coordinate system attached to the base of the platform is given by $(0, x_P, y_P, z_P)$ and the one attached to the beam by $(0, x_B, y_B, z_B)$. The rotation matrices read $R_0^P = R_z(\varphi_P)$, $R_P^B = R_z(\varphi_B)$, and $R_0^B = R_0^P R_P^B = R_z(\varphi_P + \varphi_B)$, where

$$R_z(\phi) = \begin{bmatrix} \cos(\phi) & -\sin(\phi) & 0 \\ \sin(\phi) & \cos(\phi) & 0 \\ 0 & 0 & 1 \end{bmatrix}.$$

The system's potential energy is given by

$$E_{\text{pot}}^{\text{sim}} = \frac{1}{2} k_t (\Delta s_1^2 + \Delta s_2^2) + mgl_G \cos(\varphi_P + \varphi_B), \quad (3)$$

where k_t is the translational spring constant, and

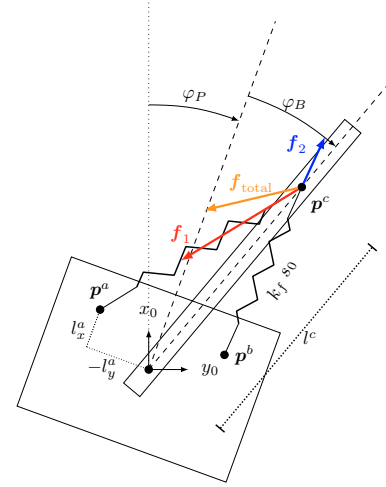
$$\Delta s_1 = \|\mathbf{p}_0^c - \mathbf{p}_0^a\|_2 - s_0 \quad (4a)$$

$$\Delta s_2 = \|\mathbf{p}_0^c - \mathbf{p}_0^b\|_2 - s_0 \quad (4b)$$

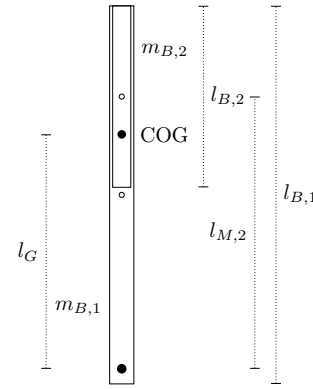
describe the elongation of the first and the second spring, respectively. Therein, s_0 denotes the length of a relaxed spring. The kinetic energy consists of the rotational energy of the platform and beam, i.e.,

$$E_{\text{kin}} = \frac{1}{2} J_{P,zz} \dot{\varphi}_P^2 + \frac{1}{2} J_{B,zz} (\dot{\varphi}_P + \dot{\varphi}_B)^2 \quad (5)$$

with the moments of inertia $J_{P,zz}$ and $J_{B,zz}$ of the platform and the beam, respectively. Energy dissipation is



(a) Rotary flexible joint coordinates, lengths and spring forces.



(b) Beam parameters with (longer) main arm and load arm.

Fig. 2. Schematic overview of geometric relations and conventions for the rotary flexible joint with an example configuration of forces acting due to the first (red) and second (blue) spring with total force (orange) acting on the beam.

given by $R = \frac{1}{2} d_P \dot{\varphi}_P^2$, where d_P is a positive damping constant. Note that damping for the beam is assumed to be negligible¹. The DC motor's momentum reads $\boldsymbol{\tau} = [0, 0, K_g \tau_m]^\top$ where K_g is the gear ratio and $\tau_m = k_b \eta_m \eta_g i$ with the motor constant k_b , the motor efficiency coefficient η_m , the gear efficiency coefficient η_g . The motor current i is given by $i = (u - k_m \dot{\varphi}_P)(R_m)^{-1}$, considering that the movements of the mechanical system are slow compared to the rate of change of the current (Kokotovic et al., 1986). Finally, the generalized, non-conservative forces induced by the DC motor read

$$\mathbf{Q}^{nc} = (J(\mathbf{q}))^\top \boldsymbol{\tau} = \begin{bmatrix} \frac{\nu(u - k_m \dot{\varphi}_P)}{R_m} \\ 0 \end{bmatrix} \quad (6)$$

with the geometric manipulator Jacobian $J(\mathbf{q})$ and $\nu = K_g k_b \eta_m \eta_g$.

2.2 Model Simplification

The mathematical model obtained with formulating the potential energy by means of the translational spring deflections leads to a very cumbersome model. Therefore,

¹ This assumption ensures that the system is/remains differentially flat.

consider the total exerted force of the springs acting on the beam $\mathbf{f}_{\text{total}} = \mathbf{f}_1 + \mathbf{f}_2$, see Fig. 2a, where

$$\mathbf{f}_1 = -\frac{\mathbf{p}_P^c - \mathbf{p}_P^a}{\|\mathbf{p}_P^c - \mathbf{p}_P^a\|_2} k_t \Delta s_1. \quad (7)$$

and \mathbf{f}_2 analogously with \mathbf{p}_P^a replaced with \mathbf{p}_P^b and Δs_1 replaced with Δs_2 . From this force the resulting moment, or generalized force with generalized coordinate² $q = \varphi_B$, is given by

$$[0, 0, Q(\varphi_B)]^\top = (R_P^B \mathbf{p}_P^c) \times \mathbf{f}_{\text{total}} \quad (8)$$

such that $Q_c(\varphi_B) = [-l^c \sin(\varphi_B), l^c \cos(\varphi_B), 0] \mathbf{f}_{\text{total}}$. A first-order Taylor polynomial around $\varphi_B = 0$ yields $Q(\varphi_B) \approx Q(0) + \frac{\partial Q}{\partial \varphi_B}(0) \varphi_B = -k_r \varphi_B$, where $Q(0) = 0$, and

$$k_r = -\frac{\partial Q}{\partial \varphi_B}(0) = -\left(\frac{2 k_t l^c l_x^a s_0}{\sqrt{(l_y^a)^2 + (l^c - l_x^a)^2}} - \frac{2 k_t (l^c)^2 (l_y^a)^2 s_0}{((l_y^a)^2 + (l^c - l_x^a)^2)^{3/2}} - 2 k_t l^c l_x^a \right). \quad (9)$$

Thus, a relationship between the translational spring stiffness k_t and the rotational spring model k_r is obtained. With this, the potential energy can be simplified using the torsion spring model, i.e.,

$$E_{\text{pot}}^{\text{ctrl}} = \frac{1}{2} k_r \varphi_B^2 + m g l_G \cos(\varphi_P + \varphi_B). \quad (10)$$

Finally, the (simplified) nonlinear model can be expressed mathematically in the form

$$\dot{\mathbf{x}} = \mathbf{f}(\mathbf{x}) + \mathbf{g}(\mathbf{x})u, \quad t > 0, \quad \mathbf{x}(0) = \mathbf{x}_0, \quad (11)$$

where $\mathbf{x} = [\varphi_P, \omega_P, \varphi_B, \omega_B]^\top$ and

$$\mathbf{f}(\mathbf{x}) = \begin{bmatrix} \frac{\omega_P}{R_m d_P \omega_P - R_m k_r \varphi_B + k_m \nu \omega_P} \\ \frac{J_{Pzz} R_m}{\omega_B} \\ f_4 \end{bmatrix}, \quad (12a)$$

$$\mathbf{g}(\mathbf{x}) = \begin{bmatrix} 0 \\ \frac{\nu}{J_{Pzz} R_m} \\ 0 \\ -\frac{\nu}{J_{Pzz} R_m} \end{bmatrix}^\top. \quad (12b)$$

The expression for f_4 can be found in Appendix A.

2.3 Differential Flatness

For a differentially flat system there exists a (fictitious) output $\lambda(\mathbf{x})$ such that (Fliess et al., 1995)

$$\mathbf{x} = \boldsymbol{\theta}_x(\lambda, \dot{\lambda}, \dots, \lambda^{(\beta-1)}) \quad (13a)$$

$$u = \boldsymbol{\theta}_u(\lambda, \dot{\lambda}, \dots, \lambda^{(\beta)}). \quad (13b)$$

The dynamical system (11) is differentially flat with flat output $\lambda(\mathbf{x}) = y = \varphi_P + \varphi_B$. This can be verified by means of the relative degree of the system for which

$$L_g L_f^k \lambda(\mathbf{x}) = 0, \quad \text{for } k = 0, \dots, r-2 \quad (14a)$$

$$L_g L_f^{r-1} \lambda(\mathbf{x}) \neq 0 \quad (14b)$$

with $r = n_x$ must hold. With this,

$$\mathbf{z} = \begin{bmatrix} z_1 \\ \vdots \\ z_{n_x} \end{bmatrix} = \boldsymbol{\Phi}(\mathbf{x}) = \begin{bmatrix} \lambda(\mathbf{x}) \\ L_f \lambda(\mathbf{x}) \\ \vdots \\ L_f^{n_x-1} \lambda(\mathbf{x}) \end{bmatrix} \quad (15)$$

² This is a valid assumption if only the spring forces are investigated since, for a torsion spring, this force only depends on the beam angle.

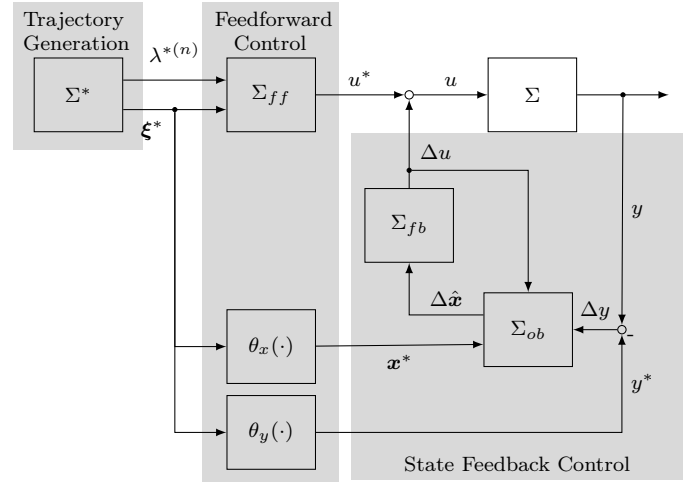


Fig. 3. Schematic structure of the flatness-based two degrees of freedom control with dynamic output control.

transforms (11) into the Brunovsky normal form and the state and input parameterizations are given by

$$\mathbf{x} = \boldsymbol{\theta}_x(\cdot) = \boldsymbol{\Phi}^{-1}(\mathbf{z}) \quad (16a)$$

$$u = \boldsymbol{\theta}_u(\cdot) = \frac{-L_f^{n_x} \lambda(\mathbf{x}) \circ \boldsymbol{\Phi}^{-1}(\mathbf{z}) + \lambda^{(n_x)}}{L_g L_f^{n_x-1} \lambda(\mathbf{x}) \circ \boldsymbol{\Phi}^{-1}(\mathbf{z})}, \quad (16b)$$

respectively (see Adamy, 2014, Sec. 5.3.4.), which are stated explicitly in Appendix B.

3. TWO DEGREES OF FREEDOM CONTROL

In this section, the 2DOF controller as depicted in Fig. 3 is discussed in detail. The control loop consists of the trajectory generation Σ^* , the feedforward control Σ_{ff} , the state feedback controller Σ_{fb} , the state difference observer Σ_{ob} , and the real system Σ , i.e., the rotary flexible joint.

Remark 1. Note that the 2DOF control design is essentially an exact feedforward linearization according to Hagenmeyer and Delaleau (2003). Alternatively, the classical nonlinear feedback linearization according to Isidori (1995) is conceptually simpler, however, the 2DOF structure allows the feedforward control to be calculated offline and also allows to analyze the effort that the state feedback controller spends on compensating model uncertainties and disturbances independently from the feedforward control and, therefore, is also an indicator of the accuracy of the model.

3.1 Trajectory Generation

The target trajectory for the flat output is designed to fulfill the boundary conditions

$$\lambda^*(t_0) = \lambda_R(t_0), \quad \dot{\lambda}^*(t_0) = \dots = \lambda^{*(\beta)}(t_0) = 0, \quad (17a)$$

$$\lambda^*(t_1) = \lambda_R(t_1), \quad \dot{\lambda}^*(t_1) = \dots = \lambda^{*(\beta)}(t_1) = 0. \quad (17b)$$

A suitable β times differentiable trajectory for the flat output $\lambda^* \in C^\beta([t_0, t_1])$ is defined by

$$\lambda^* = \lambda_R(t_0) + (\lambda_R(t_1) - \lambda_R(t_0)) \sum_{i=\beta+1}^{2\beta+1} p_i \left(\frac{t-t_0}{t_1-t_0} \right)^i \quad (18)$$

for $t \in [t_0, t_1]$, where $T = t_1 - t_0$ is the transition time. For $t = t_0$, $\beta + 1$ boundary conditions are already fulfilled

by (17a). To fulfill the remaining boundary conditions, the coefficients p_i are determined by

$$p_i = \frac{(-1)^{i-\beta-1} (2\beta + 1)!}{i\beta! (i - \beta - 1)! (2\beta + 1 - i)!} \quad (19)$$

for $i = \beta + 1, \dots, 2\beta + 1$. Finally, the trajectory generator is given by

$$\Sigma^* : \begin{bmatrix} \dot{\boldsymbol{\xi}}^* \\ \lambda^{*(\beta)} \end{bmatrix}, \quad (20)$$

with $\boldsymbol{\xi}^* = [\lambda^*, \dots, \lambda^{*(\beta-1)}]^\top$.

3.2 Feedforward Control

The feedforward control is obtained by means of the flat parameterization, i.e.

$$\Sigma_{ff} : u^* = \theta_u \left(\lambda^*, \dot{\lambda}^*, \dots, \lambda^{*(n_x)} \right) \quad (21)$$

along with the $\beta = n_x$ times differentiable target trajectory λ^* introduced in (20).

3.3 State Feedback Controller

The feedforward control can be extended with any stabilizing controller Hagenmeyer and Delaleau (2003). In this study, a PI state feedback controller compensates for model uncertainties and disturbances and stabilizes the system around the target trajectory. To this end, the state (difference) vector $\Delta \mathbf{x} = \mathbf{x} - \mathbf{x}^*$ is augmented with the integral of the tracking error, whose time derivative is given by $\Delta \dot{x}_i = -\mathbf{c}^\top(t) \Delta \mathbf{x}$, where $\mathbf{c}^\top(t) = \frac{\partial h}{\partial \mathbf{x}}|_{(\mathbf{x}^*, u^*)}$. Furthermore, the flat parameterization (13) is used to obtain (\mathbf{x}^*, u^*) , i.e., the nominal target system trajectory \mathbf{x}^* for the feedforward input u^* given by (21) to linearize the nonlinear system (11), which yields the augmented linear time-varying (LTV) system

$$\frac{d}{dt} \begin{bmatrix} \Delta \mathbf{x} \\ \Delta x_i \end{bmatrix} = \underbrace{\begin{bmatrix} A(t) & \mathbf{0} \\ -\mathbf{c}^\top(t) & 0 \end{bmatrix}}_{\bar{A}(t)} \underbrace{\begin{bmatrix} \Delta \mathbf{x} \\ \Delta x_i \end{bmatrix}}_{\Delta \mathbf{x}} + \underbrace{\begin{bmatrix} \mathbf{b}(t) \\ 0 \end{bmatrix}}_{\bar{\mathbf{b}}(t)} \Delta u \quad (22a)$$

where $A(t) = \frac{\partial \mathbf{f}}{\partial \mathbf{x}}|_{(\mathbf{x}^*, u^*)}$, $\mathbf{b}(t) = \frac{\partial \mathbf{g}}{\partial u}|_{(\mathbf{x}^*, u^*)}$. Since the feedforward control is assumed to achieve a state trajectory sufficiently close to \mathbf{x}^* the LTV system constitutes a good approximation of the error dynamics. Based on this, the state feedback controller is expressed mathematically as

$$\Sigma_{fb} : \Delta u = -\mathbf{k}^\top(t) \begin{bmatrix} \Delta \mathbf{x} \\ \Delta x_i \end{bmatrix}, \quad (23)$$

where $\mathbf{k}^\top(t)$ is obtained using the Ackermann formula (Ackermann, 1972; Wiberg, 1971)

$$\mathbf{k}^\top(t) = \frac{1}{\bar{b}_{n_x}(t)} \sum_{k=0}^{n_x+1} p_k M_{\bar{A}}^k \mathbf{w}^\top(t), \quad (24)$$

with $M_{\bar{A}}^k \mathbf{w}^\top(t) = M_{\bar{A}}(M_{\bar{A}}^{(k-1)} \mathbf{w}^\top(t))$, $M_{\bar{A}}^1 \mathbf{w}^\top(t) = \dot{\mathbf{w}}^\top(t) + \mathbf{w}^\top(t) \bar{A}(t)$, $M_{\bar{A}}^0 = \mathbf{w}^\top(t)$, p_i , $i = 0, \dots, n_x + 1$ coefficients of a Hurwitz polynomial, and $\bar{b}_{n_x}(t)$ is a degree of freedom. The vector $\mathbf{w}^\top = [0, \dots, \bar{b}_{n_x}(t)] S^{-1}(\bar{A}(t), \bar{\mathbf{b}}(t))$, where $S(\bar{A}(t), \bar{\mathbf{b}}(t))$ is the Kalman controllability matrix. Therefore, the controller gain (24) places the eigenvalues of

the closed-loop dynamics $\dot{\mathbf{z}} = A_g \mathbf{z} = (\bar{A}(t) - \bar{\mathbf{b}}(t) \mathbf{k}^\top(t)) \mathbf{z}$ of the transformed state \mathbf{z} to have poles with strictly negative real parts and, thus, exponentially stabilizes the error $\Delta \mathbf{x}$ around the origin.

3.4 State (Difference) Observer

The state information is reconstructed by means of a nonlinear Luenberger-type observer see, e.g., Rothfuss (1997), of the form

$$\Sigma_{ob} : \begin{cases} \Delta \dot{\hat{\mathbf{x}}} = \mathbf{f}(\hat{\mathbf{x}}) - \mathbf{f}(\mathbf{x}^*) + \mathbf{g}(\hat{\mathbf{x}})u - \mathbf{g}(\mathbf{x}^*)u^* \\ \quad + \mathbf{l}(t)(\Delta y - \Delta \hat{y}), \\ \Delta \hat{y} = h(\hat{\mathbf{x}}) - h(\mathbf{x}^*). \end{cases} \quad (25)$$

Similar to the state feedback gain, the observer gain is calculated based on the linearization around the target trajectory (but not using the augmented system) and is calculated for the resulting LTV observer error dynamics using

$$\mathbf{l}(t) = \frac{1}{\tilde{c}_{n_x-1}(t)} \sum_{k=0}^{n_x} p_k N_A^k \mathbf{v}(t). \quad (26)$$

Therein, $N_A^k \mathbf{v}(t) = N_A(N_A^{(k-1)} \mathbf{v}(t))$, $N_A^1 \mathbf{v}(t) = -\dot{\mathbf{v}}(t) + A(t) \mathbf{v}(t)$, $N_A^0 = \mathbf{v}(t)$, p_i , $i = 0, \dots, n_x$ coefficients of a Hurwitz polynomial, and $\tilde{c}_{n_x-1}(t)$ is a degree of freedom. The vector $\mathbf{v} = O^{-1}(\mathbf{c}^\top(t), A(t)) [0, \dots, \tilde{c}_{n_x-1}]^\top$, where $O(\mathbf{c}^\top(t), A(t))$ is the Kalman observability matrix.

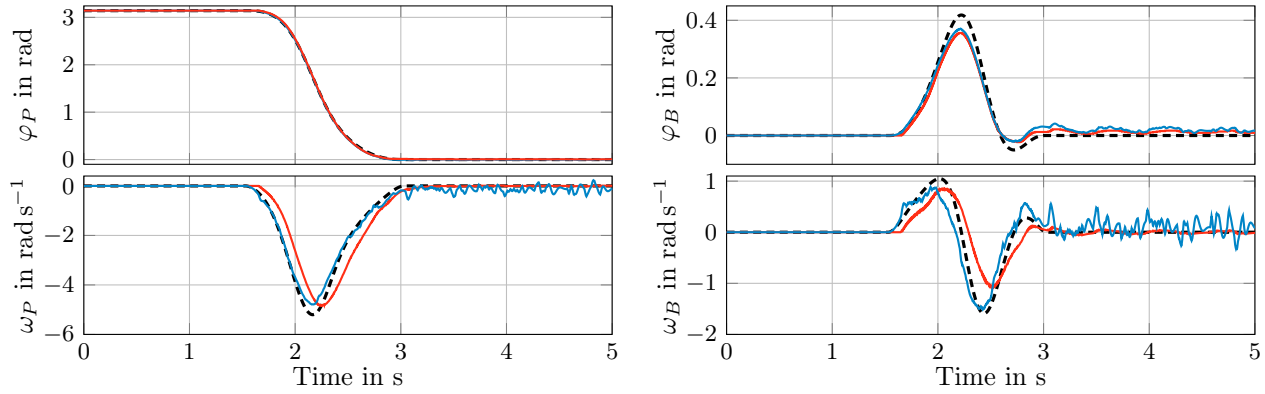
4. EXPERIMENTAL RESULTS

The presented 2DOF flatness-based control scheme is illustrated by means of an experimental setup using MATLAB/Simulink and dSPACE. The desired controller and observer poles of the closed-loop system, target trajectory coefficients, and system parameters are summarized in Tab. 1. The estimate of the rotational spring constant according to (9) yields $k_r = 0.3959 \text{ N m}$, whereas an experimental identification based on the natural frequency results in

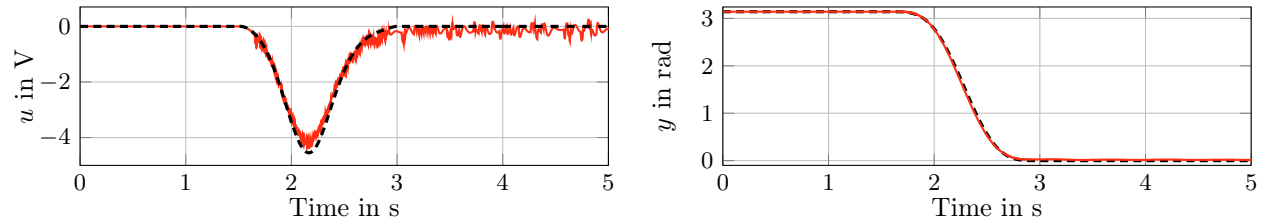
$$k_r \approx \omega_0^2 J_{B,zz} = 0.4739 \text{ N m} \quad (27)$$

with $\omega_0 = 11.7929 \text{ rad s}^{-1}$. In the experiment, we compare the controller performance of the calculated value (9) with the experimentally-obtained value. To this end a swing up of the rotary flexible joint starting with $\mathbf{x}(0) = [\pi, 0, 0, 0]^\top$ and finishing at $\mathbf{x}(T) = [0, 0, 0, 0]^\top$ is realized in $T = 1.5 \text{ s}$. The feedforward control and the trajectory generation approximately realize this transition while the state feedback controller in conjunction with the observer stabilize the reference trajectory.

In Fig. 4a, the nominal (dashed black), measured (red) and estimated (blue) states can be seen. Since $y = \varphi_P + \varphi_B$ is measured, the respective estimates for φ_P and φ_B are accurate while the estimated velocities ω_P and ω_B deviate from the filtered velocities. The angular velocities cannot be measured directly and a discrete FIR filter is used to obtain the depicted values. This also explains why the measured (or filtered) velocities lag behind their respective estimates. In Fig. 4b on the left, the feedforward input u^* is shown (dashed black) along with the total input $u = u^* + \Delta u$ (red) with state feedback control Δu and k_r according to (9). It is evident that the feedforward control



(a) System state nominal \mathbf{x}^* (dashed black), i.e., calculated by means of the flat parameterization and the feedforward system input u^* , measured state (red), and estimated state $\hat{\mathbf{x}}$ (blue).



(b) Feedforward system input u^* (dashed black) and total input $u = u^* + \Delta u$ (red) on the left, and desired output y^* (dashed black) and measured output (red) on the right.

Fig. 4. Experimental results of the rotary flexible joint swing up with measured and estimated system state (top) and system input (bottom) with k_r determined using (9).

is sufficiently accurate since the feedback controller applies little effort to stabilize the trajectory error and, thus, justifies the 2DOF control scheme that utilizes the model knowledge to design the feedforward control in contrast to a classical feedback linearization that does not distinguish between feedforward and feedback control. Furthermore, the desired output (dashed black) is also shown in Fig. 4b on the right with the measured output (red). As can be seen the overall 2DOF controller performance achieves the swing-up in the specified transition time. Note that the experimental results with k_r according to (27) are qualitatively similar to the results with k_r according to (9) and are therefore omitted for clarity. The same holds true for a comparison with a controller that implements a classical feedback linearization according to Isidori (1995).

5. CONCLUSION

In this contribution, a flatness-based 2DOF control scheme is presented and implemented using a vertically-mounted rotary flexible joint that performs a swing-up. This experiment allows to study a multitude of different concepts from modeling and identification to control and observer design using nonlinear and linear methods. The contribution focuses on simplification of the mathematical model and gives an illustrative experimental example of a nonlinear 2DOF control design of the rotary flexible joint. The 2DOF controller includes a flatness-based feedforward control and a state feedback controller that stabilizes the error from the feedforward trajectory. The stabilizing controller relies on full state information that is reconstructed by means of a Luenberger-type observer. Therefore, this experiment is also a good example for students to understand the necessity of observers in state feedback control design.

Both the stabilizing controller and the observer rely on a linearization of the nonlinear system around the desired trajectory using the flat system parameterization. The feedback and observer gains are designed such that the time variance of the linearized system is compensated and pole placement achieves the desired transient behavior. The 2DOF control scheme is illustrated by means of an experimental setup. All in all, this experiment gives insight to many different nonlinear and linear control theory concepts and offers students the possibility to experiment with a variety of modifications and extensions w.r.t. the stabilizing controller and the observer design. For example, the pole placement of the state feedback controller can be modified to achieve a different transient behavior, or can be replaced by a PID controller to investigate loop shaping.

Appendix A. NONLINEAR SYSTEM DYNAMICS

The last entry in the drift vector field of the system dynamics reads

$$f_4 = \frac{1}{J_{B,zz} J_{P,zz} R_m} \left(J_{B,zz} R_m d_P \omega_P - J_{B,zz} R_m \cdot k_r \varphi_B - J_{P,zz} R_m k_r \varphi_B + J_{B,zz} k_m \nu \omega_P + J_{P,zz} R_m g l_G m_{B1} \sin(\varphi_B + \varphi_P) + J_{P,zz} R_m g l_G m_{B2} \sin(\varphi_B + \varphi_P) \right). \quad (\text{A.1})$$

Appendix B. FLAT PARAMETERIZATION

The flat parameterization of the states and inputs read

Group	Name	Symbol	Value
Spring(s)		l^c	0.0768 m
	fix-point(s)	l_x^a	0.0251 m
		l_y^a	0.0316 m
	translational stiffness	k_t	112 N/m
	rotational stiffness	k_r (9) k_r (27)	0.3959 N m 0.4739 N m
	relaxed length	s_0	0.03 m
Beam	length from joint to middle of load arm	$l_{M,2}$	0.2206 m
	length from joint to center of gravity	l_G	0.1720 m
	moment of inertia	$J_{B,zz}$	0.0034 kg m ²
	mass of main arm	$m_{B,1}$	0.064 kg
	mass of load arm	$m_{B,2}$	0.030 kg
	length of main arm	$l_{B,1}$	0.298 m
	length of load arm	$l_{B,2}$	0.156 m
Platform	moment of inertia	$J_{P,zz}$	0.0019 kg m ²
	damping	d_P	0.015 kg m ² /s
Motor	resistance	R_m	2.53 Ω
	current-torque	k_b	0.0077 kg m ² /(A s ²)
	back-emf	k_m	0.0077 V/(rad s)
	gear ratio	K_g	70
	gearbox efficiency	η_g	0.895
	motor efficiency	η_m	0.69
Target Trajectory	polynomial coefficients	$[p_5, p_6, p_7]$	[126, -420, 540]
		$[p_8, p_9]$	[-315, 70]
	degree	β	4
	boundary value(s)	$\lambda_R(t_0)$ $\lambda_R(t_1)$	π rad 0 rad
	transition time	T	1.5 s
Controller	desired poles	-	[-15, 16, 17, 18, 19]
Observer	desired poles	-	[-30, 35, 40, 45]

Table 1. Parameters of the rotary flexible joint, the DC motor, trajectory generation, controller, and observer.

$$\begin{aligned} \mathbf{x} &= \theta_x(\lambda, \dot{\lambda}, \dots, \lambda^{(3)}) \\ &= \frac{1}{k_r} \begin{bmatrix} k_r \lambda - gl_G m_{B1} \sin(\lambda) + gl_G m_{B2} \sin(\lambda) - J_{B,zz} \ddot{\lambda} \\ J_{B,zz} \lambda^{(3)} + k_r \dot{\lambda} - gl_G m_{B1} \cos(\lambda) \dot{\lambda} - gl_G m_{B2} \cos(\lambda) \dot{\lambda} \\ - J_{B,zz} \ddot{\lambda} + gl_G m_{B1} \sin(\lambda) + gl_G m_{B2} \sin(\lambda) \\ gl_G m_{B1} \cos(\lambda) \dot{\lambda} - J_{B,zz} \lambda^{(3)} + gl_G m_{B2} \cos(\lambda) \dot{\lambda} \end{bmatrix} \\ \mathbf{u} &= \theta_u(\lambda, \dot{\lambda}, \dots, \lambda^{(4)}) \\ &= k_r \nu (J_{B,zz} R_m d_P \lambda^{(3)} + J_{B,zz} k_m \nu \lambda^{(3)} + R_m d_P k_r \dot{\lambda} \\ &\quad + J_{B,zz} J_{P,zz} R_m \lambda^{(4)} + k_m k_r \nu \dot{\lambda} + J_{B,zz} R_m k_r \ddot{\lambda} \\ &\quad + J_{P,zz} R_m k_r \ddot{\lambda} - R_m g k_r l_G m_{B1} \sin(\lambda) - R_m g \\ &\quad \cdot k_r l_G m_{B2} \sin(\lambda) - R_m d_P gl_G m_{B1} \cos(\lambda) \dot{\lambda} \\ &\quad - R_m d_P gl_G m_{B2} \cos(\lambda) \dot{\lambda} - g k_m l_G m_{B1} \nu \cos(\lambda) \dot{\lambda} \\ &\quad - g k_m l_G m_{B2} \nu \cos(\lambda) \dot{\lambda} + J_{P,zz} R_m gl_G m_{B1} \\ &\quad \cdot \sin(\lambda) \dot{\lambda}^2 + J_{P,zz} R_m gl_G m_{B2} \sin(\lambda) \dot{\lambda}^2 \\ &\quad - J_{P,zz} R_m gl_G m_{B1} \cos(\lambda) \ddot{\lambda} - J_{P,zz} R_m gl_G m_{B2} \cos(\lambda) \ddot{\lambda}) \end{aligned}$$

respectively.

REFERENCES

- Ackermann, J. (1972). Der Entwurf linearer Regelungssysteme im Zustandsraum. *at - Automatisierungstechnik*, 20, 297–300.
- Adamy, J. (2014). *Nichtlineare Systeme Und Regelungen*. Springer Vieweg, Berlin, 3rd edition.

- Akyuz, I., Yolacan, E., Ertunc, H., and Bingul, Z. (2011). PID and state feedback control of a single-link flexible joint robot manipulator. In *2011 IEEE International Conference on Mechatronics*, 409–414. Istanbul, Turkey.
- Bilal, H., Yao, W., Guo, Y., Wu, Y., and Guo, J. (2017). Experimental validation of fuzzy PID control of flexible joint system in presence of uncertainties. In *2017 36th Chinese Control Conference (CCC)*, 4192–4197. Dalian, China.
- Book, W.J. (1983). Recursive Lagrangian Dynamics of Flexible Manipulator Arms via Transformation Matrices. *IFAC Proceedings Volumes*, 16(19), 5–17.
- Dharavath, P.K. and Ohri, J. (2021). Optimized Control Design of LQR for Flexible Joint Manipulator. volume 760 of *Lecture Notes in Electrical Engineering*, 261–269. Springer, Singapore.
- Didam, M.E., Agee, J.T., Jimoh, A.A., and Tlale, N. (2012). Nonlinear control of a single-link flexible joint manipulator using differential flatness. In *2012 5th Robotics and Mechatronics Conference of South Africa*, 1–6. Johannesburg, South Africa.
- Fliess, M., Levine, J., Martin, P., and Rouchon, P. (1995). Flatness and defect of non-linear systems: Introductory theory and examples. *International Journal of Control*, 61(6), 1327–1361.
- Hagenmeyer, V. and Delaleau, E. (2003). Exact feedforward linearization based on differential flatness. *International Journal of Control*, 76, 537–556.
- Isidori, A. (1995). *Nonlinear Control Systems*. Communications and Control Engineering. Springer, London.
- Kokotovic, P.V., Khalil, H.K., and O'Reilly, J. (1986). *Singular Perturbation Methods in Control: Analysis and Design*. Number 25 in Classics in Applied Mathematics. SIAM, Philadelphia, USA, 1st edition.
- Markus, E., Agee, J., Jimoh, A.G., Tlale, N., and Zafer, B. (2012). Flatness based Control of a 2 DOF Single Link Flexible Joint Manipulator. In *2nd International Conference on Simulation and Modeling Methodologies, Technologies and Applications*, 437–442.
- Markus, E.D. (2016). Experimental validation on flatness based control of flexible robot arm. In *2016 PRASA-RobMech*, 1–5. IEEE, Stellenbosch, South Africa.
- Quanser (2012). Rotary Flexible Joint - User Manual. Technical report.
- Riviere, C., Wei Tech Ang, and Khosla, P. (2003). Toward active tremor canceling in handheld microsurgical instruments. *IEEE Transactions on Robotics and Automation*, 19(5), 793–800.
- Rothfuss, R. (1997). *Anwendung Der Flachheitsbasierten Analyse Und Regelung Nichtlinearer Mehrgrößensysteme*, volume 8 of *VDI Fortschrittsberichte*.
- Rsetam, K., Cao, Z., and Man, Z. (2020). Cascaded-Extended-State-Observer-Based Sliding-Mode Control for Underactuated Flexible Joint Robot. *IEEE Transactions on Industrial Electronics*, 67(12), 10822–10832.
- Sendrescu, D., Bujgoi, G., and Chintescu, D. (2020). Control of a Rotary Flexible Joint Experiment based on Reinforcement Learning. In *2020 21th International Carpathian Control Conference (ICCC)*, 1–5.
- Wiberg, D.M. (1971). *State Space and Linear Systems*. McGraw-Hill, New York.